

A new method for evaluating the plastic properties of materials through instrumented frictional sliding tests

S.C. Bellemare^a, M. Dao^b, S. Suresh^{b,*}

^a Structural Engineering and Structural Mechanics Division, Simpson, Gumpertz and Heger, Waltham, MA 02453, USA

^b Department of Materials Science and Engineering, Massachusetts Institute of Technology, Cambridge, MA 02139, USA

Received 3 February 2010; received in revised form 30 July 2010; accepted 31 July 2010

Abstract

Frictional normal contact probing methods involving instrumented, depth-sensing indentation can be used to estimate the mechanical properties of small-volume structures and materials such as thin films and components of micro-electro-mechanical systems. This paper describes a new method for estimating the plastic properties, i.e. the yield strength and strain hardening exponent, of ductile materials from the topography of scratches formed by a conical tip during an instrumented, depth-sensing frictional sliding test. The proposed reverse analysis (or inverse analysis) uses dimensionless functions derived from computational simulations to extract plastic properties from an instrumented scratch response performed on a standard, commercially available instrument. Sensitivity analysis indicates that an experimental error of 5% in the scratch hardness or the pile-up height induces an error of <22% in the estimated strain hardening exponent. Laboratory experiments illustrate how two aluminum alloy tempers of the same indentation hardness have significantly different pile-up as a result of different strain hardening. Comparative results between the frictional sliding test and traditional tensile tests showed reasonable agreement for a total of 11 metallic alloys evaluated. These results confirm the potential usefulness of the proposed method as an engineering tool to probe plastic properties of small-volume materials and confined structures where it is difficult to obtain reliable estimates of mechanical properties by other means.

© 2010 Acta Materialia Inc. Published by Elsevier Ltd. All rights reserved.

Keywords: Scratch test; Elasto-plastic properties; Small-volume materials and devices; Reverse algorithm; Friction

1. Introduction

Mechanical tests such as the tensile test are employed extensively to determine the yield strength and ductility of metals. These tests are appropriate when a sufficient volume of homogeneous material is available for determination of mechanical properties using traditional methods. These techniques for extracting mechanical properties, however, are impossible or inappropriate when the elasto-plastic responses of small-volume ductile materials are needed. Components can be too small or have local gradients in properties which are too steep for testing using traditional means. Examples of such components or systems include free-formed devices, thin films, micro-electro-

mechanical system structures, composites, coatings, forgings and welds.

Contact mechanics has evolved as an attractive method for probing material properties of thin films and small-volume structures because testing can be performed at multiple local length scales using polished metallographic sections. In recent years, researchers have developed methods of estimating the yield strength and ductility of metals using instrumented, frictionless normal indentation [1–4]. The so-called forward problem predicts an indentation response, typically obtained as the variation in indentation normal force P as a function of the depth of penetration of the indenter tip into the material surface h from a given set of elasto-plastic properties. By contrast, the reverse algorithm estimates elasto-plastic properties from depth-sensing indentation response (i.e. from a knowledge of the loading and unloading portions of the

* Corresponding author. Tel.: +1 617 253 3291.

E-mail address: ssuresh@mit.edu (S. Suresh).

P vs. h curves obtained experimentally) using algorithms derived from computational simulations. In the indentation forward algorithms, small errors in the elasto-plastic properties only lead to small uncertainties in predicting indentation response.

The developed indentation reverse algorithms in general provide reasonably accurate predictions of the reduced modulus of elasticity (E^*), but these predicting functions are relatively sensitive to small experimental errors in evaluating yield strength and hardening [2,4,5]. Often, indentation test results with two or more sharp indenter geometries are needed to provide accurate and unique predictions of elasto-plastic properties [5–8], while, in general, experimental results obtained from a single spherical indenter geometry can ensure unique extraction of plastic properties [5,9]. The representative plastic strain for deformation under a sharp indenter is in the range 3–8% for a conical tip with a total included angle of 140.6° , depending on the method of analysis [2].

Frictional sliding in steady state is an alternative loading condition where the instrument induces a lateral displacement of a tip under a constant normal load. Different analytical models [10], test data [11–13] and computational models [14–21] have been developed for the steady-state flow of material. Analytical models have several limitations, including difficulties in resolving the local strain field and in accounting for the effects of plastic strain hardening of the material on the scratch response. Previous test results indicated a lack of correlation between the scratch hardness and the indentation hardness [12].

Recent research [18,20] showed that moderate changes in the strain hardening of metals greatly influences the topography of scratches obtained from a frictional sliding test, and that the representative plastic strain for a conical tip with an included angle of 140.6° is in the range 15–34%, depending on the combination of yield strength and strain hardening exponent. Previous results [18,20,21] showed that the representative plastic strain during instrumented frictional sliding tests is on the order of 5–10 times larger than that in instrumented indentation tests. A detailed comparison of the plastic deformation characteristics between frictional sliding and indentation can be found in Ref. [21]. Stress and strain distribution with or without the presence of plasticity gradient during the instrumented frictional sliding test under the indenter were obtained and reported in Ref. [21]. These recent results also indicated that the overall coefficient of friction in frictional sliding has a limited dependence on the elasto-plastic properties. A set of dimensionless functions were derived from extensive computational simulations for predicting frictional sliding response from a given set of elasto-plastic properties and the adhesive friction coefficient [20], which effectively established the forward analysis method for the frictional sliding test (or the instrumented scratch test). The instrumented frictional sliding test, similar to the indentation test, can be performed at a penetration depth as small as 5–10 nm [22,23], although at the same penetration depth

the instrumented frictional sliding experiment would require a considerably larger sampling area and volume (on the order of $20\times$ compared with the indentation test to achieve steady state) because of the sliding motion. The related validation experiments were performed at depths deep enough to avoid the penetration size effect [18,20].

This paper describes and evaluates a new reverse algorithm for the frictional sliding test for estimating the local plastic properties of metallic alloys. This engineering method uses the elastic properties of the material, the scratch hardness and the normalized pile-up height as inputs for calculations using dimensionless functions. The resulting output is an estimate of the yield strength and the strain hardening exponent of the metallic alloy. This technique leads to yield strength results similar to those obtained from instrumented indentation with a single indenter, but the estimate of the strain hardening exponent is relatively more reliable and accurate, as shown by both sensitivity analysis and experiments using several different metallic alloys.

2. Materials and methods

2.1. Frictional sliding test

Fig. 1 illustrates a frictional sliding test to obtain the input data. The surface must be free of contaminants and have a roughness whose scale (e.g. asperity height and width) is small compared with the depth of penetration of the indenter. The indenter used is a cone shape with an included angle of 140.6° . This axisymmetric tip geometry is selected because the projected area of the indenter impression as a function of the indentation depth is the same as that for the standard Berkovich or Vickers indenter tips. For the purpose of a frictional sliding test, sharper tips (with a smaller total included angle) lead to a greater risk of chip formation, but more blunted tips reduce the magnitude of the plastic deformation. Other tip geometries would require a re-evaluation of the numerical functions described here.

After the tip is positioned at the targeted location on the sample, the instrument applies a normal load, and the indenter penetrates the surface. Subsequently, the tip moves relative to the sample, or vice versa, to form a permanent scratch under a constant normal load. As previously described [18], the penetration depth initially increases and then decreases until it reaches steady state, in which the width of the residual scratch and the amount of material pushed on each side of the indenter are constant. In general, this steady-state travel distance is between two and three times the width of the scratch.

On completion of the scratch, surface profilometry provides the average peak-to-peak width of the scar $2a_r$, where a_r is the residual contact radius, and the average residual pile-up height h_p . The residual scar depth h_r is either obtained directly by surface profilometry, if the scanning

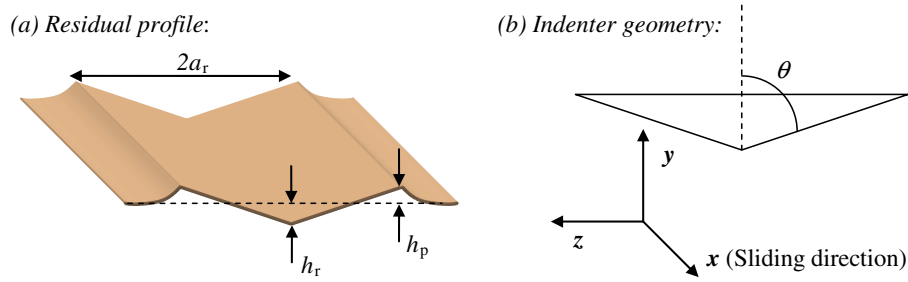


Fig. 1. (a) A section of a residual scratch profile where the pile-up height (h_p), the residual penetration depth (h_r) and the contact radius (a_r) are indicated, and (b) a schematic view of a conical indenter with an apex angle θ . Also shown is the coordinate system for the analysis.

tip is sharper than the scratching tip, or indirectly using the tip geometry, if the scanning tip is the same as the scratching tip. These data provide the normalized pile-up height r_p and the scratch hardness H_S using the traditional definition of hardness [24–26]:

$$r_p = \frac{h_p}{h_r} \quad (1)$$

and

$$H_S = \frac{2P}{\pi a_r^2} \quad (2)$$

where P is the applied normal load. In the absence of size effects on material properties, these two parameters are independent of the applied load or depth of penetration, which simplifies the analysis and the predicting equations.

During the frictional sliding test, the control unit of the indenter can monitor the lateral contact force using beam deflection, capacitors or other methods. These data provide insight into the plastic deformation process, but the engineering method described here did not make particular use of these additional data. As previously described [20], the overall lateral contact force is influenced by material plastic properties, but it is also driven by the intrinsic coefficient of adhesive friction. Therefore, small changes in the intrinsic coefficient of adhesive friction or typical measurement variability could lead to errors in the predictions.

2.2. Predictive methodology

Fig. 2 summarizes the proposed frictional sliding reverse analysis algorithm. The method is based on the influence of the plastic flow properties on the scratch hardness and the normalized pile-up height. The material constitutive behavior is isotropic with linear elasticity, which is captured by an exponential plastic hardening law for the true flow stress

$$\sigma = \sigma_y \left(1 + \frac{E}{\sigma_y} \varepsilon_p \right)^n \quad (3)$$

where ε_p is the true equivalent plastic strain, σ_y is the initial yield strength, E is Young's modulus of the material, and n is the plastic strain hardening exponent. The elastic contributions from the material and the indenter can be simplified using the reduced modulus [25].

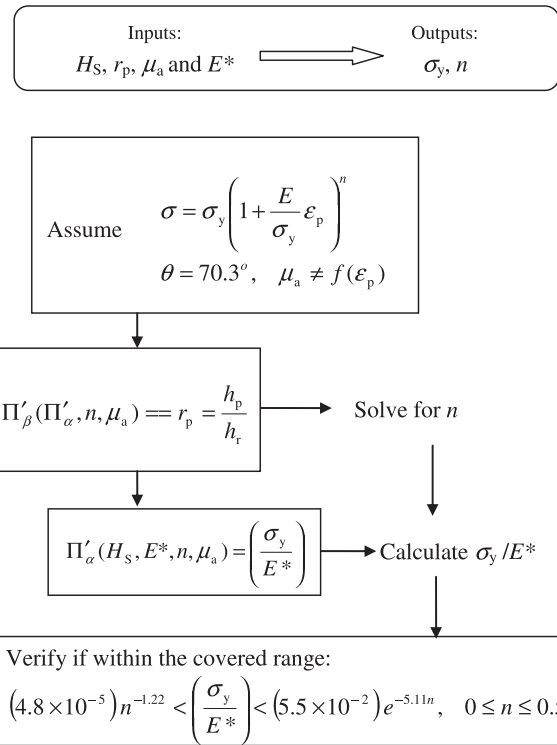


Fig. 2. Outline of steps involved in the frictional sliding reverse analysis algorithm.

$$E^* = \left[\frac{(1 - \nu^2)}{E} + \frac{(1 - \nu_i^2)}{E_i} \right]^{-1} \quad (4)$$

where E_i and ν_i are Young's modulus and Poisson's ratio of the indenter, respectively. For polycrystalline diamond, the typical material of choice for the indenter tip, $E_i = 1100$ GPa and $\nu_i = 0.07$ are assumed.

For frictional sliding contact, independent functions can be written for independent quantities such as the scratch hardness H_S , the pile-up height h_p and the overall friction coefficient μ_{tot} . By making the quantities dimensionless and using the Π theorem, the functions can be evaluated numerically and then used for any specific material condition within the solution space. For a fixed cone angle θ of 70.3° , the finite element results from a detailed parametric study provided the following dimensionless functions [18,20]

$$\Pi_\alpha = \left(\frac{H_S}{\sigma_y} \right) = [\alpha 1(n) + n \Gamma_{\alpha 1}(\mu_a)] \left(\frac{\sigma_y}{E^*} \right)^{[\alpha 2(n) + \Gamma_{\alpha 2}(\mu_a)]} \quad (5)$$

$$\begin{aligned} \Pi_\beta &= \frac{h_p}{h_r} = r_p \\ &= \Pi_{\beta,RP}(n) \Gamma_{\beta,RP}(\mu_a) \left/ \left[1 + \left(\frac{\sigma_y}{X_\beta(n) \Gamma_{X\beta}(\mu_a) E^*} \right)^{p_\beta(n)} \right] \right. \end{aligned} \quad (6)$$

and

$$\begin{aligned} \Pi_\gamma &= \left(\frac{F_t}{P} \right) = \mu_{tot} = \mu_a + (\Pi_{\gamma,RP} \Gamma_{\gamma,RP}(\mu_a) - \mu_a) \left/ \left[1 + \left(\frac{\sigma_y}{X_\gamma(n) \Gamma_{X\gamma}(\mu_a) E^*} \right)^{p_\gamma(n)} \right] \right. \end{aligned} \quad (7)$$

where the subscript RP indicates the value of the function at the limit of rigid plastic properties, and the variable F_t is for the overall lateral force. All numerical closed-form solutions to these sub-functions are listed in the [Appendix A](#). The proposed frictional sliding reverse algorithm is developed based on the dimensionless functions Π_α and Π_β . Π_γ , which relates to the friction response, is included here for completeness. Π_γ could be used to solve the system of equations for a third unknown such as the frictional coefficient μ_a or the reduced modulus E^* , but it is not used here for the prediction because, as described in Section 2.1, their inclusion would not improve accuracy, but instead could possibly reduce accuracy. E^* can be easily obtained using the same instrument with the indentation test. The frictional coefficient μ_a can be obtained using a procedure described in Ref. [20].

The algorithm requires the following information:

- Coefficient of adhesive friction μ_a can be measured experimentally using a nearly elastic contact between the same material and a spherical tip [20], or other methods.
- Elastic properties for the tip and the material to compute E^* can be obtained from material data table and the literature, from tensile tests or from instrumented indentation.

The method is based on the following assumptions:

- The indenter is a nearly perfect cone with an apex angle of 70.3°, which corresponds to a total included angle of 140.6°.
- Incremental theory of plasticity is valid, and there are no size effects within the region of experimental measurement.
- The material plastic flow behavior is isotropic, and it follows the power law per Eq. (3).

Under these conditions, the reverse algorithm outlined in [Fig. 2](#) uses the above dimensionless functions in the following form:

$$\begin{aligned} \Pi'_\alpha(H_S, E^*, n, \mu_a) &= \left(\frac{\sigma_y}{E^*} \right) \\ &= \left[\left(\frac{H_S}{E^*} \right) / (\alpha 1(n) + n \Gamma_{\alpha 1}(\mu_a)) \right]^{[1/(1+\alpha 2(n) + \Gamma_{\alpha 2}(\mu_a))]} \end{aligned} \quad (8)$$

and

$$\begin{aligned} \Pi'_\beta(\Pi'_\alpha, n, \mu_a) &= r_p = \frac{h_p}{h_r} \\ &= \Pi_{\beta,RP}(n) \Gamma_{\beta,RP}(\mu_a) \left/ \left[1 + \left(\frac{\Pi'_\alpha}{X_\beta(n) \Gamma_{X\beta}(\mu_a)} \right)^{p_\beta(n)} \right] \right. \end{aligned} \quad (9)$$

To solve this system numerically, Π'_α is inserted into Π'_β , which allows Π'_β to be solved numerically by varying n to match the experimental value of r_p . As shown in Section 3, the value of r_p steadily decreases with increasing n , simplifying the solution procedure. The value of n obtained is then inserted in Π'_α to determine σ_y/E^* . To solve this system of equations numerically, the equations can be implemented in a calculus spreadsheet by reserving columns for the outputs and for each sub-function of n or μ_a . A single iteration loop is needed to solve Π'_β for n . The range of conditions used to determine Π'_α and Π'_β using finite element simulations is

$$\begin{aligned} (4.8 \times 10^{-5})n^{-1.22} < \left(\frac{\sigma_y}{E^*} \right) < (5.5 \times 10^{-2})e^{-5.11n}, \\ \text{where } 0 \leq n \leq 0.5 \end{aligned} \quad (10)$$

This range of material properties covers a wide variety of engineering materials, but exceptional cases may fall outside this range. A solution that does not verify the above inequality (Eq. (10)) could be inaccurate, because it would be based on extrapolated regression functions.

2.3. Experimental materials and properties

Materials tested for verification of the proposed method included nickel, copper and aluminum alloys. A high purity 2000 series aluminum alloy AA 2524-T3 sheet metal product 0.8 mm thick was selected to generate two materials with the same indentation hardness, but different microstructures (obtained from the Aluminum Company of America (Alcoa) Technical Center, Alcoa Center, Pennsylvania). Tensile specimens machined from these sheets met the dimensional requirements of ASTM E-8 [27] and had the tensile axis oriented at 45° to the rolling direction in order to probe the average properties. The specimens were heat-treated at 190 ± 5 °C for different aging times. The hardness and tensile properties measured after aging are provided in [Table 2](#). The stress–strain curves corrected for machine/specimen compliance were consistent with the permanent elongation of the specimens obtained by marking and length variation measurements.

Cut sections for the frictional sliding tests were polished mechanically with the rolling direction normal to the plane. The final surface roughness was characterized using a Q-Scope 250 (Quesant Instrument Corporation, Santa Cruz, CA) atomic force microscope in non-contact mode.

Prior work provided detailed experimental description and mechanical properties of the nickel alloys [18] and copper alloys [20] used for the verification of the engineering

Table 1
Sensitivity analysis for the reverse algorithm.

	Δ on σ_y for H_S		Δ on n for H_S		Δ on σ_y for h_p/h_r		Δ on n for h_p/h_r	
	+5%	-5%	+5%	-5%	+5%	-5%	+5%	-5%
$n \leq 0.1$	7.9	-7.7	-11.8	12.1	14.4	-12.1	-21.9	21.1
$0.1 < n \leq 0.2$	10.8	-10.0	-15.2	15.8	13.3	-12.8	-15.5	16.9
$0.2 < n \leq 0.35$	11.3	-10.9	-11.3	10.8	12.8	-11.8	-12.6	13.3
$0.35 < n \leq 0.5$	20.3	-11.6	-11.2	3.8	12.3	-11.3	-8.1	7.9

method described here. In all cases, the surface roughness of the specimens was estimated to be <10 nm.

2.4. Experimental frictional test apparatus and parameters

All frictional sliding tests were with a conical diamond indenter with an included angle of 140.6° and a tip radius of $2 \mu\text{m}$. For the conditions of penetration depth investigated ($\sim 5\text{--}15 \mu\text{m}$), the scale of experimentation was sufficiently large to consider this indenter perfectly conical and to neglect the penetration size effect. The wear of the diamond tip was not significant in terms of tip radius blunting. Testing was performed on a commercially available nanoindentation test system (NanotestTM, Micro Materials Ltd., Wrexham, UK) under constant normal load P , at a tip velocity of $10 \mu\text{m s}^{-1}$ and over a total distance of $1500 \mu\text{m}$, which was sufficient to attain steady-state conditions after $\sim 300 \mu\text{m}$ and then generate a region of valid steady-state profile.

After the experiment, a series of at least 30 cross-sectional residual profiles were obtained over the steady-state sliding regime using a Tencor P10 profilometer (KLA-Tencor, San Jose, CA). The profilometer was equipped with a conical diamond probe which had an included tip angle of 90° and a tip radius of $2 \mu\text{m}$. A typical procedure involved the generation of five parallel scratches on each sample, followed by 6–10 transverse scans going across these scratches. The resulting data were treated with a computer algorithm to correct for surface curvature, to isolate the individual profiles and to calculate the profile characteristics.

3. Results and discussion

3.1. Predicting functions for reverse analysis

The solution method is fully explained with two equations (Eqs. (8) and (9)) and two unknowns: the initial yield strength σ_y and the strain hardening exponent n . Fig. 3 illustrates the dependence of each equation on the unknowns for a fixed adhesive friction coefficient $\mu_a = 0.15$. The ordinate is plotted on a logarithmic scale to improve the visual representation of the yield strength (σ_y/E^*) for soft materials. All curves have a steadily decreasing slope, but the slopes for the r_p curves are more negative than the slopes for the σ_y/E^* curves. Because of this difference in slope, a curve of fixed r_p intersects a curve of fixed H_S/E^* at a single point.

The coordinates for this intersection point correspond to the solution for n and σ_y , the unknowns. With this approach, the solution for a given set of input variables is unique within the parameter space studied. The chart in Fig. 3 provides a direct approximation for n and σ_y using elastic properties and frictional sliding test data, but solving Eqs. (8) and (9) numerically provides more precision in the prediction.

Eq. (8) for σ_y/E^* provides additional insight into the dependence of the scratch hardness on plastic properties. Fig. 4 shows stress–strain curves for materials with the same normalized scratch hardness ($H_S/E^* = 0.2$) using Eq. (8) with an adhesive friction coefficient $\mu_a = 0.15$. This friction coefficient was obtained through a procedure discussed elsewhere [20]. The curves intersect at values of plastic strain $>25\%$. It is shown that the normalized pile-up height r_p can vary significantly between metals of same normalized scratch hardness.

3.2. Sensitivity analysis

The solution varies with the experimental values of H_S and r_p . Table 1 shows how a variation of 5% in the input parameters influences the solution to Eqs. (8) and (9). The values reported in each cell of this table were the maximum found for all permitted values of σ_y/E^* . The effect of

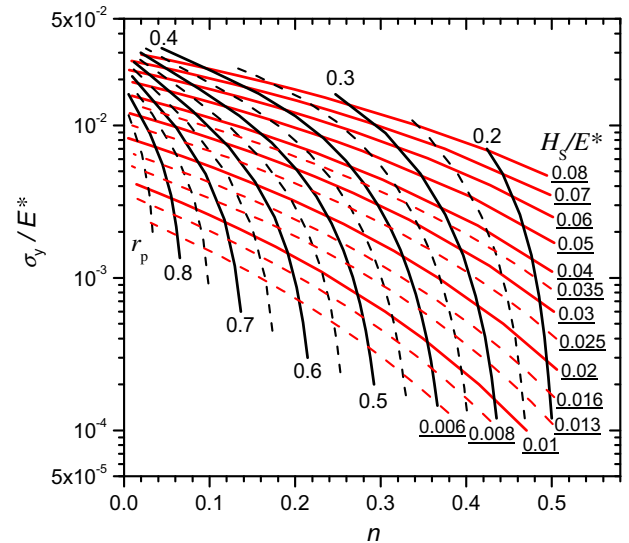


Fig. 3. Chart for estimating the strain hardening exponent and the normalized initial yield strength from the normalized scratch hardness and the normalized pile-up height ($\mu_a = 0.15$).

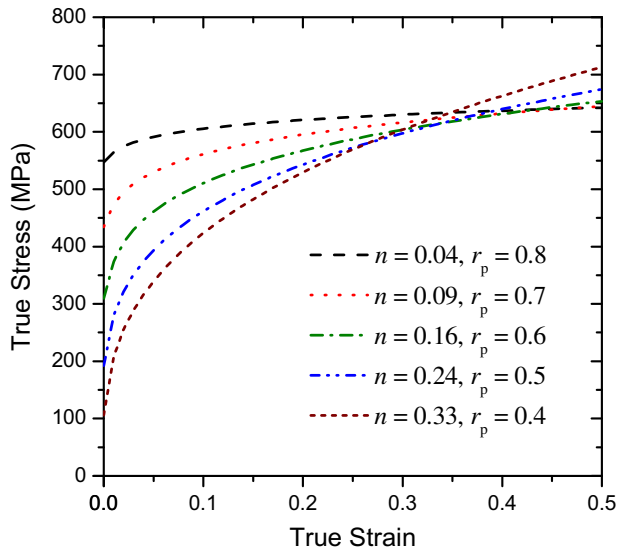


Fig. 4. Flow stress curves of materials with the same normalized scratch hardness H_S/E^* of 0.02 ($\mu_a = 0.15$).

a 5% variation is at most 22%. For example, the table indicates that a variation of 5% in an input parameter will change the prediction of the strain hardening exponent in the range 0.125–0.175 if the true strain hardening exponent is 0.15. This level of variability is adequate for many engineering applications.

The predictive method is based on known and fixed values of the friction coefficient μ_a , whose determination is subject to experimental uncertainty; it may vary with surface preparation. To test the effect of this variation, Fig. 5 shows the variation in the solution for an average value of $\mu_a = 0.14$ and a variation of $\pm 25\%$. The result shows that r_p and H_S/E^* remain within 6% of their original values for $\mu_a = 0.14$. Therefore, variability in the estima-

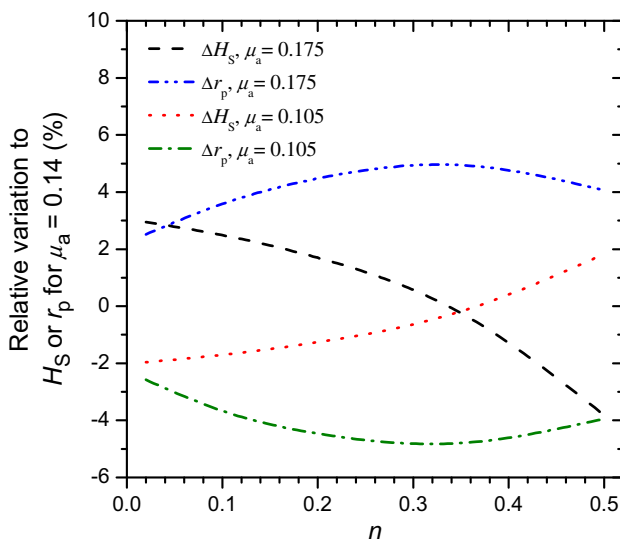


Fig. 5. Variation in the value of hardness H_S and normalized pile-up height r_p for different values of friction coefficient μ_a .

tion of μ_a is less critical for the overall accuracy of the proposed method than the variability in the input parameters σ_y/E^* and r_p .

3.3. Experimental verification

Laboratory testing confirmed the trends predicted by the dimensionless functions. Fig. 6 compares the residual cross-sectional profiles from frictional sliding experiments on two aluminum alloys with the same indentation hardness. One specimen was in T3 temper (quenched and naturally aged), while the other was over-aged to the same indentation hardness. The profiles from the as-received specimen present a lower and blunted pile-up, which is primarily due to the higher strain hardening exponent. These

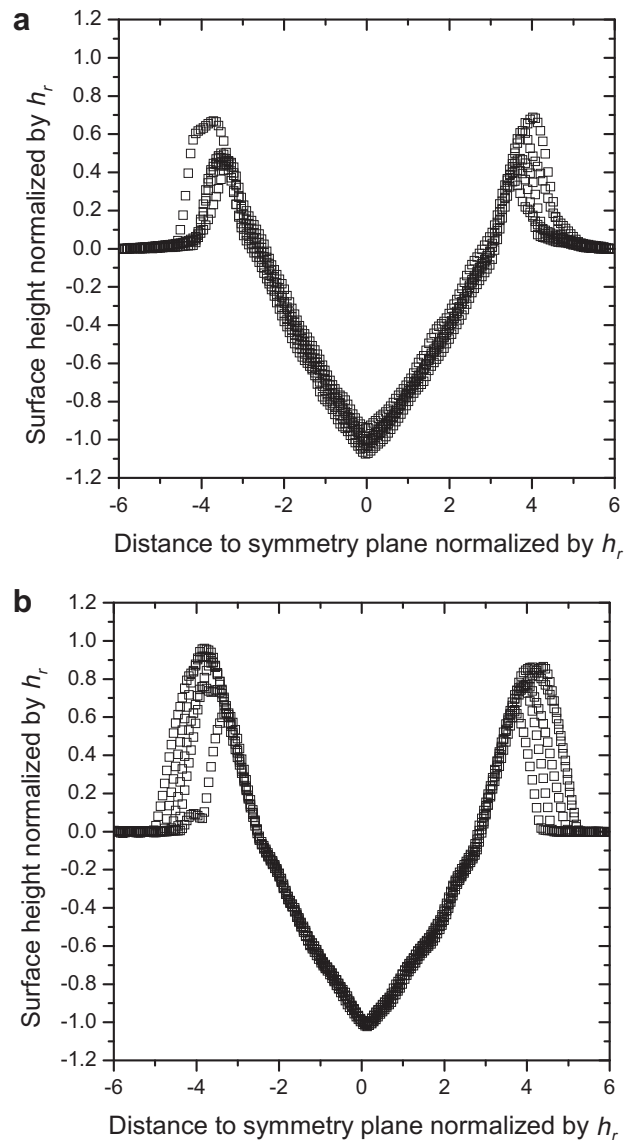


Fig. 6. Residual cross-sectional profiles for the aluminum alloy in the: (a) as-received and (b) over-aged conditions. The sliding direction is normal to the plane. In each case, five individual scratch profiles are shown to illustrate the scatter in the experimental results.

Table 2

Comparison between the predictions from the reverse analysis and the experimental values; the data for pure Cu, Cu–Zn and pure Ni are from previous work [18,20].

	Experimental		Predicted properties		Properties from tension		Variation between predicted and measured properties (%)	
	H_S (GPa)	h_p/h_r	$\sigma_{0.2\%}$ (MPa)	n	$\sigma_{0.2\%}$ (MPa)	n	$\sigma_{0.2\%}$	n
Al (as-received)	1.3	0.54	220	0.18	180	0.21	18	–17
Al (aged)	1.1	0.79	330	0.08	370	0.05	–12	38
Cu (450 °C)	0.66	0.7	145	0.13	135	0.13	7	0
Cu (600 °C)	0.62	0.57	44	0.27	58	0.23	–32	15
Cu (700 °C)	0.60	0.51	28	0.29	35	0.28	–25	3
Cu–Zn (450 °C)	1.13	0.44	45	0.35	59	0.32	–31	9
Cu–Zn (600 °C)	0.95	0.3	15.5	0.41	12.9	0.44	17	–7
Cu–Zn (700 °C)	0.81	0.28	7.0	0.45	7.8	0.45	–11	0
Ni (nc)	4.42	0.84	1600	0.02	1723	0.02	–8	0
Ni (ufc)	2.63	0.76	850	0.06	804	0.07	5	–17
Ni (mc)	1.35	0.63	170	0.19	201	0.18	–18	5

differences in the relative shape of the profiles could translate into a different resistance to tribological damage. A lower and more blunted profile may reduce the amount of material removal in a subsequent tribological event.

Laboratory testing also verified the quantitative predictive capability of the method. The predicted results were compared with tensile test data on pure nickel, pure copper and a single phase brass alloy, in addition to the aluminum alloy presented in this study. These materials constituted a wide range of grain sizes. Table 2 presents the predictions from the reverse analysis along with tensile test data. The difference between the experimental measurements and the predictions from the proposed method is generally <20%. Only two cases out of 22 had a variation >20%. In those two cases, the variation remained <40%. These experimental findings are consistent with the results from the sensitivity analysis using the dimensionless functions Π'_α and Π'_β .

Both the frictional sliding tests and the dimensionless functions showed that the scratch hardness and the pile-up height correlate with the strain hardening exponent. As a result, the method described here can provide a range and/or a comparative ranking of materials with respect to their strain hardening exponent.

4. Concluding remarks

From an analysis of dimensionless functions and the experimental verification described in the present paper, the following conclusions are drawn:

1. Two materials with the same indentation hardness can form significantly different scratch hardness and pile-up behavior during frictional sliding.
2. A new reverse (or inverse) algorithm is proposed for extracting plastic properties from instrumented scratch response using dimensionless functions derived from computational simulations. It is demonstrated that the plastic properties of metals can be predicted using fric-

tional sliding results obtained from commercially available instrumented, depth-sensing scratch test equipment. Provided that the elastic properties and contact properties are known, the normalized hardness and the normalized pile-up height are sufficient to determine the plastic strain hardening exponent and the initial yield strength.

3. The method proposed here is sensitive to experimental errors. A variation of 5% in the value of the normalized hardness or the normalized pile-up height can result in an error of up to 22% in the prediction of the strain hardening exponent.
4. Experimental errors associated with variations in the adhesive coefficient of friction between the indenter tip and the material have a relatively smaller effect on the predicted values for the yield strength and the strain hardening exponent.
5. Using this frictional sliding test, the yield strength and the strain hardening exponent can be extracted uniquely and with a reasonable accuracy without requiring the use of two or more indenter geometries. Here, known values of E^* and μ_a are prerequisites. The reduced modulus E^* can be easily obtained using the same instrument with the indentation test. The frictional coefficient μ_a can be obtained using a procedure described in Ref. [20], but a precise determination is not critical. It is also noted that Π_γ in Eq. (7) could be used to solve the system of equations for a third unknown such as the frictional coefficient μ_a or the reduced modulus E^* .
6. Using the same instrumentation and calibration, the frictional sliding test can be used to identify small variations in strain hardening exponent.
7. The frictional sliding test can also be performed in conjunction with standard instrumented, depth-sensing, frictionless normal indentation on the same instrument, with one or more tip geometries, to enhance significantly the accuracy of the extracted elasto-plastic material properties.

Acknowledgements

The authors would like to acknowledge the financial support from the ONR Grant N00014-08-1-0510, as well as a research Grant provided by Schlumberger Limited. S.S. and M.D. further acknowledge support from the Advanced Materials for Micro and NanoSystems Programme of the Singapore-MIT Alliance (SMA) and the Singapore-MIT Alliance for Research and Technology (SMART).

Appendix A. Numerical functions

$$\begin{aligned} \Pi'_z(H_S, E^*, n, \mu_a) &= \left(\frac{\sigma_y}{E^*}\right) \\ &= \left[\left(\frac{H_S}{E^*}\right) / (\alpha 1(n) + n\Gamma_{z1}(\mu_a))\right]^{[1/(1+\alpha 2(n)+\Gamma_{z2}(\mu_a))]} \end{aligned} \quad (8)$$

with

$$\alpha 1(n) = 3.32 - 5.79n + 2.8n^2 \quad (8.1)$$

$$\Gamma_{z1}(\mu_a) = 0.12 - 0.64/[1 + e^{30(\mu_a - 0.1)}] \quad (8.2)$$

$$\alpha 2(n) = 0.07 - 1.283n + 0.248n^2 \quad (8.3)$$

$$\Gamma_{z2}(\mu_a) = 0.006 - 0.0278/[1 + e^{25(\mu_a - 0.1)}] \quad (8.4)$$

$$\begin{aligned} \Pi'_\beta(\Pi'_z, n, \mu_a) &= r_p = \frac{h_p}{h_r} = \Pi_{\beta,RP}(n)\Gamma_{\beta,RP}(\mu_a) / \\ &\left[1 + \left(\frac{\Pi'_z}{X_\beta(n)\Gamma_{X\beta}(\mu_a)}\right)^{p_\beta(n)}\right] \end{aligned} \quad (9)$$

with

$$\Pi_{\beta,RP}(n) = 0.904 - 1.684n + 1.987n^2 - 2.722n^3 \quad (9.1)$$

$$\Gamma_{\beta,RP}(\mu_a) = 0.909 + 0.627\mu_a \quad (9.2)$$

$$\begin{aligned} X_\beta(n) &= 0.0378 - 0.2129n + 1.145n^2 - 3.34n^3 \\ &+ 3.54n^4 \end{aligned} \quad (9.3)$$

$$\Gamma_{X\beta}(\mu_a) = 0.651 + 1.21\mu_a + 7.61\mu_a^2 \quad (9.4)$$

$$p_\beta(n) = -0.68 \ln(n + 0.02) \quad (9.5)$$

References

- [1] Oliver WC, Pharr GM. *J Mater Res* 1992;7(6):1564–83.
- [2] Dao M, Chollacoop N, Van Vliet KJ, Venkatesh TA, Suresh S. *Acta Mater* 2001;49(19):3899–918.
- [3] Cheng YT, Cheng CM. *Mater Sci Eng R* 2004;44(4–5):91–149.
- [4] Gouldstone A, Chollacoop N, Dao M, Li J, Minor AM, Shen Y-L. *Acta Mater* 2007;55(12):4015–39.
- [5] Lan H, Venkatesh TA. *Philos Mag* 2007;87(30):4671–729.
- [6] Bucaille JL, Stauss S, Felder E, Michler J. *Acta Mater* 2003;51(6):1663–78.
- [7] Chollacoop N, Dao M, Suresh S. *Acta Mater* 2003;51(13):3713–29.
- [8] Cao YP, Lu J. *Acta Mater* 2004;52(5):1143–53.
- [9] Collin JM, Mauvoisin G, Bartier O, El Abdi R, Pilvin P. *Mater Sci Eng A* 2009;501(1–2):140–5.
- [10] Williams JA. *Tribol Int* 1996;29(8):675–94.
- [11] Black AJ, Kopalinsky EM, Oxley PLB. *Wear* 1988;123(1):97–114.
- [12] Brookes CA, Green P, Harrison PH, Moxley B. *J Phys D: Appl Phys* 1972;5:1284–93.
- [13] Jardret V, Zahouani H, Loubet JL, Mathia TG. *Wear* 1998;218(1):8–14.
- [14] Bucaille JL, Felder E, Hochstetter G. *Wear* 2001;249(5–6):422–32.
- [15] Bucaille JL, Felder E. *Philos Mag A* 2002;82(10):2003–12.
- [16] Fang L, Cen Q, Sun K, Liu W, Zhang X, Huang Z. *Wear* 2005;258(1–4 SPEC ISS):265–74.
- [17] Felder E, Bucaille JL. *Tribol Int* 2006;39(2):70–87.
- [18] Bellemare S, Dao M, Suresh S. *Int J Solids Struct* 2007;44(6):1970–89.
- [19] Wredenberg F, Larsson PL. *J Mech Mater Struct* 2007;2(3):573–94.
- [20] Bellemare SC, Dao M, Suresh S. *Mech Mater* 2008;40(4–5):206–19.
- [21] Prasad A, Dao M, Suresh S. *Acta Mater* 2009;57(2):511–24.
- [22] Bellemare SC. Micro and nano mechanics of materials response during instrumented frictional sliding. PhD thesis, Department of Materials Science and Engineering, Massachusetts Institute of Technology; 2006.
- [23] Beake BD, Bell GA, Goodes SR, Pickford NJ, Smith JF. *Surf Eng* 2010;26(1–2):37–49.
- [24] Tabor D. *The hardness of metals*. Oxford: Clarendon Press; 1951.
- [25] Johnson KL. *Contact mechanics*. London: Cambridge University Press; 1985.
- [26] Fischer-Cripps AC. *Introduction to contact mechanics*. New York: Springer; 2000.
- [27] ASTM Committee E28. *ASTM E-8: Standard test methods for tension testing of metallic materials*. West Conshohocken (PA): ASTM International; 2004.